Energy & Environmental Science

COMMUNICATION

View Article Online
View Journal | View Issue

Cite this: *Energy Environ. Sci.*, 2014, 7, 3611

Received 16th June 2014
Accepted 9th September 2014

DOI: 10.1039/c4ee01850h

www.rsc.org/ees

Large scale, flexible and three-dimensional quasi-ordered aluminum nanospikes for thin film photovoltaics with omnidirectional light trapping and optimized electrical design†

Siu-Fung Leung,[a] Kwong-Hoi Tsui,[a] Qingfeng Lin,[a] Hongtao Huang,[b] Linfeng Lu,[b] Jia-Min Shieh,[c] Chang-Hong Shen,[c] Chin-Hung Hsu,[c] Qianpeng Zhang,[a] Dongdong Li*[b] and Zhiyong Fan*[a]

Nanostructured photovoltaics has attracted an enormous amount of attention in recent years owing to its potency for significant device performance enhancement over the conventional technologies. Nonetheless, conventional fabrication approaches for nanostructured scaffolds rely on glass or silicon substrates which are costly, brittle and have limited scalability. Meanwhile, rational design guidelines for optical and electrical performance optimization of solar cells are of urgent need for their practical applications. In this work, flexible and quasi-ordered three-dimensional (3-D) nanospike (NSP) arrays are fabricated on a reasonable large scale with well controlled geometry. Systematic investigations by experiments discovered that photovoltaic devices based on NSPs with optimal geometry can accommodate the trade-off between optical absorption and electrical performance, demonstrating a power conversion efficiency of 7.92%, which is among the highest efficiency reported for single junction a-Si:H solar cells on a flexible substrate. Furthermore, we have demonstrated the superior omnidirectional device performance by utilizing such a 3-D NSP. This unique feature is of paramount importance for practical photovoltaic applications.

Broader context

A large scale, flexible and three dimensional aluminum nanospike was fabricated by a facile and low cost anodization process. A solar cell device on the optimal morphology of NSPs showed excellent angular dependent performance and achieved a PCE of 7.92% which is among the highest single junction a-Si:H PCE reported on a flexible substrate to the best of our knowledge. Furthermore, a large scale NSP solar cell device with excellent flexibility was demonstrated which has a significant impact on flexible PV applications.

1 Introduction

Thin film photovoltaics (TF-PV) is a highly enticing alternative to the conventional crystalline silicon technology as low cost and portable energy sources owing to its substantially reduced material consumption, attractive light-weight and excellent flexibility.[1–12] Nonetheless, utilization of ultra-thin materials often limits the optical absorption of the solar cell and thus put a constraint on the performance of the TF-PV devices. Therefore, utilization of three-dimensional (3-D) nanostructures for photon management in optoelectronic devices including photovoltaic (PV) devices has become an intriguing topic.[5,10,13–37] In this case, light absorption can be significantly enhanced with a relatively thin layer of active materials and thus the minority carrier diffusion path length is not increased. Therefore, various 3-D nanostructures such as nanocones,[3,4,6,8,14,38–46] nanopillars[1,15,21,47–52] nanowells,[51,53–55] *etc.* have been explored and they have demonstrated remarkable effectiveness in improving the performance of PV devices. However, most of the 3-D nanostructured substrates employed are based on non-flexible and brittle materials such as silicon and glass.[38] More importantly, fabrication of nanotextures on these substrates normally involved costly processes such as photolithography and dry etching that hindered the large-scale and cost-effective PV panel manufacturing. On the other hand, conventional plastic flexible substrates have a relatively low melting point which greatly limits the process temperature for fabrication of high performance TF-PV devices on them.[56] Therefore, from a practical standpoint, it is of interest to develop nanotextures for advanced light management on a higher melting point substrate at low cost and on a large scale. In this regard, we have reported the fabrication of regular arrays of the 3-D nanospike (NSP) structure on flexible aluminum (Al) foils with nanoimprint in conjunction with electrochemical

[a]*Department of Electronic and Computer Engineering, Hong Kong University of Science and Technology, Clear Water Bay, Kowloon, Hong Kong, China. E-mail: eezfan@ust.hk*
[b]*Shanghai Advanced Research Institute, Chinese Academy of Sciences, 99 Haike Road, Zhangjiang Hi-Tech Park, Pudong, Shanghai 201210, China. E-mail: lidd@sari.ac.cn*
[c]*National Nano Device Laboratories (NDL), Hsinchu 30078, Taiwan, Republic of China*

† Electronic supplementary information (ESI) available: Methods for morphology characterization, optical reflectance, device performance characterization and the daily integrated power output ratio of solar cells. Figures: statistical data of NSP height and NSP PV device efficiencies. The normal incidence optical reflectance of NSPs with different morphologies; the external quantum efficiency (EQE) of a-Si:H solar cells on different morphologies of NSPs; the angular and wavelength dependent absorption spectra of solar cells on 200 V, 400 V and 600 V NSP substrates. See DOI: 10.1039/c4ee01850h

anodization.[10,47,57] It has been discovered that the regularity is beneficial in order to achieve thin films with reasonable uniformity. Meanwhile, our previous work has also demonstrated that the quasi-ordered 3-D NSPs achieved by the improved high voltage anodization without nanoimprint could efficiently capture light.[47] In fact, it is an intrinsically low cost process to fabricate quasi-ordered NSPs by natural anodization. In this work, we report single junction amorphous silicon (a-Si:H) PV devices fabricated on the quasi-ordered 3-D aluminum NSP substrates with different morphologies. Solar cells fabricated on the optimal morphology resulted in a power conversion efficiency (PCE) of 7.92% under air mass spectrum 1.5 global (AM 1.5G) illumination, which is 34% improvement over its planar counterpart and it is among the highest single junction a-Si:H PCE reported on a flexible substrate to the best of our knowledge. In addition, the trade-off between the enhanced optical absorption by a high aspect ratio nanostructure and the increased carrier recombination due to thin film uniformity issue was revealed by systematic characterization and analysis. More importantly, we have demonstrated the superior omni-directional PV performance of NSP solar cells and large scale devices with excellent flexibility which have practical significance to a wide range of PV applications including utility power generation, building integrated PV and the next generation portable electronics.

2 Experimental

2.1 Preparation of the NSP substrate

The schematic of the NSP fabrication process is displayed in Fig. 1a. First, aluminum foil was cut into 1 cm by 2 cm pieces and cleaned in acetone and isopropyl alcohol. The sheets were then electrochemically polished in a 1 : 3 (v/v) mixture of perchloric acid and ethanol for 2 min at 10 °C. The polished Al chips were anodized with voltages of 200 V, 400 V, 500 V and 600 V for 9–16 hours. The electrolyte for anodization was a mixture of citric acid, ethylene glycol, and phosphoric acid.

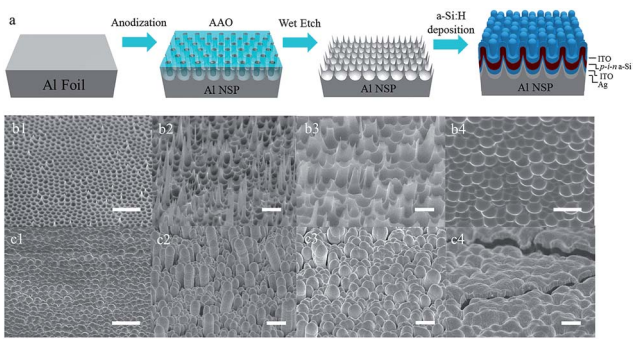

Fig. 1 Fabrication process and SEM images of the 3-D aluminum nanospike. (a) Schematic diagram of fabrication of the 3-D aluminum nanospike. (b1–b4) 45° tilted SEM images of NSPs fabricated by anodization with 200 V, 400 V, 500 V and 600 V respectively. (c1–c4) 45° tilted SEM images of a-Si:H thin film solar cells fabricated on 200 V, 400 V, 500 V and 600 V NSPs respectively (scale bars in the SEM images are 2 μm).

For an applied voltage of 200 V, the solution was 2 wt% citric acid, ethylene glycol, and 85 wt% phosphoric acid in a volume ratio of 200 : 100 : 0.5 vol%; for 400–500 V voltage, the solution was 2 : 1 vol% for the 2 wt% citric acid and ethylene glycol; while for 600 V voltage, the solution was diluted to 1 : 1 vol% for 2 wt% citric acid and ethylene glycol. A carbon rod was used as the counter-electrode during anodization. After anodization, 3-D Al NSP arrays were exposed by etching away the anodic aluminum oxide (AAO) layer with a mixture of chromium acid (1.5 wt%) and phosphoric acid (6 wt%) solutions at 63 °C for 30 minutes. After etching, the chips were cleaned with deionized-water and blown dry with air for the subsequent thin film deposition. Aluminum foil anodized with 200 V, 400 V, 500 V and 600 V led to different morphologies of NSPs and their scanning electron microscopy (SEM) images are shown in Fig. 1b1–b4 respectively. It can be observed that the pitch of NSPs (distance between the neighboring NSPs) increases with anodization voltage. Apparently, 400 V anodized aluminum has the tallest NSP structure (the highest aspect ratio), then followed by 500 V, whereas NSPs fabricated by 200 V and 600 V anodization are the shortest (lowest aspect ratio) which is consistent with our previous report.[47] The statistics of NSP height by different anodization voltages can be found in ESI Fig. S1.† On the other hand, it is known that aluminum have higher coefficient of thermal expansion (CTE) than silicon and glass. Therefore, CTE mismatch between the aluminum substrate and the solar cell thin film can cause the failure of the device. Also, aluminum diffusion at high temperature is detrimental for the a-Si:H PV device.[58] To address these issues, the top 100 nm surface of aluminum was anodized with 20 V DC, using 1.7 wt% H_2SO_4 as an electrolyte. This thin layer of aluminum oxide can serve as a buffer layer to mitigate the CTE mismatch and block the aluminum diffusion. Since it is very thin, the flexibility of the solar cell would not be affected which is proven by the results shown in Fig. 5. Meanwhile, it is worth pointing out that in our 3-D device structure, a-Si:H thin film, the top and bottom ITO layers are essentially "folded" on the substrate, which can help to release the stress/strain caused by CTE mismatch as well according to our previous report.[10]

2.2 Fabrication of a-Si:H solar cells on a 3-D NSP substrate

For a-Si:H solar cell fabrication, firstly 100 nm thick silver and 200 nm thick indium doped tin-oxide (ITO) were magnetron sputtered as the bottom contact. Subsequently, a-Si:H layers were deposited by plasma enhanced chemical vapor deposition (PECVD) with n–i–p layers of 20 nm, 350 nm and 12 nm respectively, using SiH_4 with H_2 dilution and B_2H_6 and PH_3 as P-type and N-type dopant. Finally, 3 mm diameter of the top ITO contact with a thickness of 200 nm was sputtered on the a-Si:H layer. The SEM micrographs of solar cell devices on an Al NSP substrate anodized by 200 V, 400 V, 500 V and 600 V are exhibited in Fig. 1c1–c4 respectively. Notably, morphologies of the NSPs can be retained after solar cell deposition which allows the study of morphology dependent optical absorption and PV performance.

3 Results and discussion

3.1 Optical reflectance characterization and electrical characterization of NSP-based thin-film solar cells

Fig. 2a shows the UV-Visible (UV-Vis) optical absorption spectra of the solar cells on 200–600 V NSPs from 380–720 nm wavelength which is considered as the above band-gap region of a-Si:H (~1.7 eV). UV-Vis optical reflectance spectra of planar and 200–600 V NSP substrates can be found in ESI Fig. S2.†

Evidently, optical absorption of solar cells with a NSP structure are far better than that of the planar control device which can be attributed to the effective light trapping effect by the NSP. Particularly, light absorption of the 400 V and 500 V devices is significantly higher than that of the 200 V and 600 V devices, especially for 400 V, the absorption across the entire measurement range is close to 100%. These results agree with the fact that 400 V anodization could produce a high aspect ratio of the NSP which can perform more efficient light trapping. Beside, PV performances of solar cells on different voltage NSP substrates were characterized under AM 1.5G (100 mW cm^{-2}) illumination. Current density–voltage (J–V) characteristics of them are shown in Fig. 2b. The detail performance parameters of the best devices are summarized in Table 1 and the statistical data of PV device performances can be found in Fig. S3.†

Apparently, even by introducing very short NSP structures with 200 V and 600 V anodization, PV device performances had already been improved substantially owing to the improved optical absorption especially in the long wavelength beyond 600 nm which is also evidenced by external quantum efficiency (EQE) measurement shown in Fig. S4.† As a result, current densities (J_{sc}) of 12.85 mA cm^{-2} and 11.17 mA cm^{-2} were achieved in the 200 V and 600 V devices respectively, which are 29% and 12% improved as compared to the planar counterpart with only marginal drop of open circuit voltage (V_{oc}) due to the increased surface recombination.[4] And the 200 V device achieved a PCE of 7.01% which is consistent with our previous work.[6] On the other hand, with the highest aspect ratio of the NSP, the 400 V device was expected to have the strongest light trapping capability and yield the best PV performance. Conversely, it was found that the efficiency of 400 V is unexpectedly lower than the planar control device due to the low V_{oc} and fill factor. And among all the devices, the 500 V device with the 2nd highest aspect ratio of the NSP has the highest J_{sc} of 14.08 mA cm^{-2}, with a V_{oc} of 0.914 V and a fill factor of 61%, resulted in the best PCE of 7.92% which is among the highest PCE of single junction a-Si:H being reported on flexible substrates to the best of our knowledge.

Table 1 Detail electrical parameters of NSP-based thin-film solar cells

Anodization voltage	V_{oc} (V)	J_{sc} (mA cm^{-2})	Fill factor (%)	Efficiency (%)
Planar	0.917	9.97	64.39	5.89
200 V	0.882	12.85	61.84	7.01
400 V	0.642	11.52	43.31	3.21
500 V	0.914	14.08	61.52	7.92
600 V	0.915	11.17	61.96	6.33

3.2 Solar cell morphology characterization

The above intriguing results can be understood by analyzing the cross-sectional SEM micrographs of 200–600 V devices which are shown in Fig. 3a–d respectively. In the SEM images, the relatively dark color layer represents a-Si:H and the top and bottom layers are ITO. It can be clearly seen that the a-Si:H film can be rather uniformly deposited on the 200 V, 500 V and 600 V NSPs. While in the case of 400 V devices, non-uniform deposition of a-Si:H was observed at the vertical sidewall which is owing to the shadowing effect of the plasma radical by the high aspect ratio of the NSP tip during PECVD deposition. The inset of Fig. 3b shows the cross-sectional SEM image of one of the tallest NSP tips which revealed that the a-Si:H thickness at the vertical sidewall is about 200 nm which is only ~50% of the expected thickness. This phenomenon has also been observed in our previous work in which the regular array of NSPs was reported.[10]

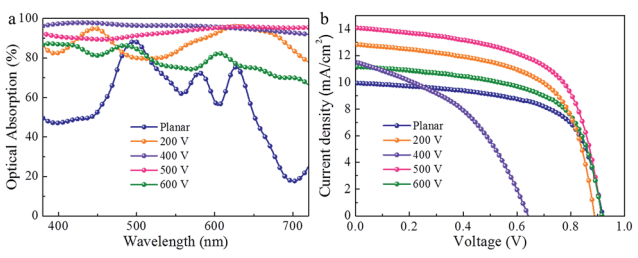

Fig. 2 Optical reflectance measurement and device performance characterization. (a) Optical reflectance spectra of the NSP solar cell with different morphologies. (b) J–V characteristics of the NSP solar cell with different morphologies.

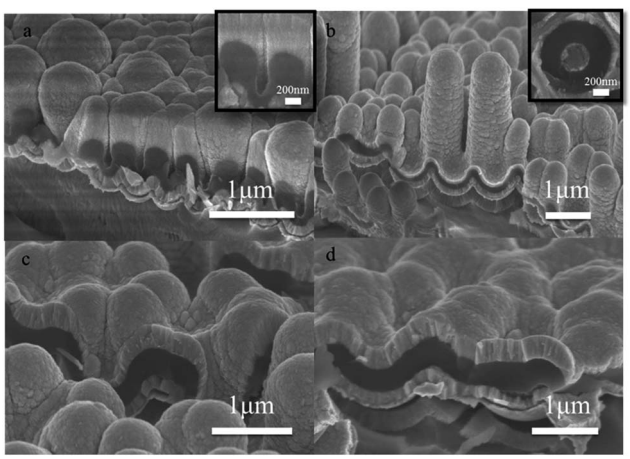

Fig. 3 Cross-sectional SEM images of solar cell devices fabricated on (a) 200 V, (b) 400 V, (c) 500 V and (d) 600 V NSPs respectively. The inset in (a) and (b) exhibit the void formed in the 200 V NSP due to relatively short pitch and cross-section of a tall NSP in the 400 V substrate indicating the non-uniform a-Si:H film deposition at the vertical NSP sidewall.

While the thickness variation of the intrinsic a-Si:H will only affect light absorption, the thinner P-doped and N-doped layers will particularly affect the internal electrical field across the junction and therefore causing extra recombination which can explain the significant drop of V_{oc} in 400 V devices.[4,54,59–61] Meanwhile, the presence of voids is observed in the 200 V devices (inset of Fig. 3a) due to the short NSP pitch. This kind of cavity structure was reported in the literature that would cause the decrease in V_{oc} and fill factor which can explain the slight drop of V_{oc} in 200 V devices.[4] In contrast, there is no void developed in the 500 V NSP due to the relatively large pitch and the absence of tall and sharp NSP tips which mitigated the non-uniform a-Si:H film deposition issue. As a result, the optimal morphology of the 500 V NSP can provide sufficient light trapping without sacrificing the electrical performance thus resulting in the best efficiency. This result suggests that the balance between optical absorption and carrier collection is of crucial importance when designing high performance 3-D nanostructured PV devices.

Besides PV performance measured with normal incident light, another important but often overlooked aspect is the omnidirectional characteristic. Since the sunlight incident angle varies throughout a day, it is a great advantage for solar cells to maintain strong absorption at an oblique angle of incident light and there were several studies reported previously regarding the efficient omnidirectional light trapping of nanowire arrays.[14,22,24] In our work, angular dependent optical absorption of solar cells on different voltage NSPs was examined. Fig. 4a and b exhibit the optical absorption spectra of solar cells on planar and 500 V NSPs for an incident angle from 0° to 60° and those of 200 V, 400 V and 600 V can be found in ESI Fig. S5.† Manifestly, the optical absorption of a solar cell on a 500 V NSP is superior compared to that on a planar control and it maintains high absorption at an oblique incident angle which is ascribed to the effectively light trapping by the 3-D NSP. Furthermore, the consistent trend can be observed in the daily integrated PV performance. Fig. 4c shows the bar chart of the daily integrated power ratio over planar to compare the power generated by solar cells on the different voltage NSP and planar throughout a sunny day and the detailed experimental procedure can be found in the ESI.† Intriguingly, solar cells on the 500 V NSP substrate can generate 32% more electricity than that on the planar substrate, followed by 19% improvement on the 200 V NSP. These results clearly demonstrate the outstanding angular dependent PV performance of solar cells on a 3-D NSP substrate which is crucial from a practical point-of-view.

On top of these, the aluminum based 3-D NSP substrate has excellent flexibility and its fabrication is highly scalable, which cannot be achieved in the conventional nanotextured substrate based on glass.[4,38]

Fig. 5a1 displays a large scale flexible 500 V NSP thin film solar cell with an active area of 12 cm^2 and achieved a PCE of 3.58% under AM 1.5G illumination which is 29% more efficient than its planar counterpart. From the J–V curves of the large scale NSP and planar solar cell displayed in Fig. 5b, it is apparent that the PCE increase is mainly due to the higher J_{sc} which implies that the light trapping capability of NSPs can be maintained under large scale fabrication. Note that the lower efficiency of the large scale device as compared with the small scale device can be attributed to the resistance of the un-optimized ITO, which is confirmed with the fill factor drop observed in Fig. 5b. To characterize the robustness of device performance upon bending, the PCE under a bending angle from 0° to 120°

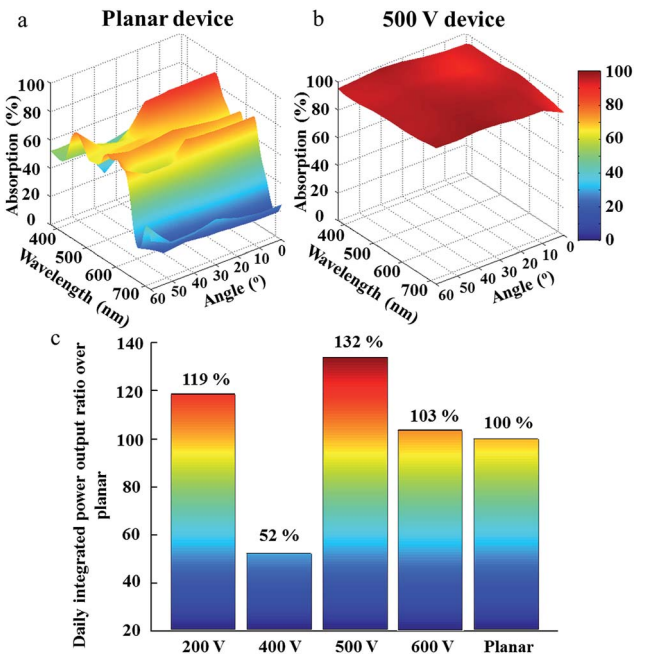

Fig. 4 Angular and wavelength dependent absorption spectra of solar cells on (a) planar and (b) 500 V NSP substrates. (c) Daily integrated power output ratio over planar control.

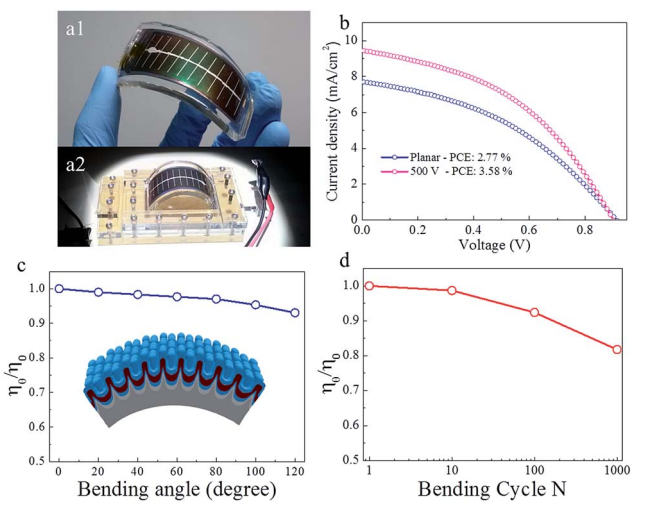

Fig. 5 Optical images of (a1) a large scale flexible NSP PV device and (a2) bending angle depending PV performance measurement setup. (b) J–V characteristic of large scale 500 V and planar PV devices. (c) Normalized efficiencies of NSP devices under bending angles up to 120° and the inset is the schematic of a bendable NSP device. (d) Relative efficiency of the NSP device after 10, 100 and 1000 bending cycles.

was measured with a customized setup as shown in Fig. 5a2 and c showing the efficiencies of a NSP device normalized with the projection area of a simulated light source with respect to bending angles up to 120°. Evidently, efficiencies only experienced a marginal drop even at high bending angle. Moreover, the reliability of NSP solar cells under bending was examined and the results are presented in Fig. 5d. The efficiency remains ~82% of the initial efficiency after 1000 cycles of bending. These results demonstrated the excellent flexibility of the aluminum based NSP substrate which is essential for flexible PV applications.

4 Conclusions

We have demonstrated thin film a-Si:H solar cells fabricated on flexible aluminum substrates with a quasi-ordered 3-D NSP substrate. The fabrication processes of Al based 3-D NSP substrates are low-cost and highly scalable. And this type of PV substrate has multiple advantages over conventional glass with textures in terms of flexibility, weight and cost-effectiveness. Our device characterization showed that, with optimal pitch and height of the NSP, a solar cell can achieve a PCE of 7.92% which outperforms the planar counterpart by 34%. More importantly, cross-sectional SEM images revealed that the optimal height of the NSP prevented excessive recombination by avoiding non-uniform a-Si:H deposition on the NSP sidewall. Furthermore, the NSP solar cell demonstrated superior angular PV performance and the daily integrated power generated is 32% higher than that of the planar control which has a significant impact on practical applications. Meanwhile, a large scale and flexible PV device with an active area of 12 cm^2 was demonstrated and exhibited excellent flexibility and reliability under bending.

Acknowledgements

This work was supported by the General Research Fund (612111 and 612113) from the Hong Kong Research Grant Council, Innovation Technology Commission (ITS117/13) and National Research Foundation of Korea funded by the Korean Government (NRF-2010-220-D00060). We also acknowledge the support from Science & Technology Commission of Shanghai Municipality (Grant No. 13DZ1106000, 14JC1492900), the National Natural Science Foundation of China (Grant No. 51102271) and Ministry of Science and Technology and National Applied Research Laboratories (NARLabs) of the Republic of China.

Notes and references

1 Z. Y. Fan, H. Razavi, J. W. Do, A. Moriwaki, O. Ergen, Y. L. Chueh, P. W. Leu, J. C. Ho, T. Takahashi, L. A. Reichertz, S. Neale, K. Yu, M. Wu, J. W. Ager and A. Javey, *Nat. Mater.*, 2009, **8**, 648–653.
2 M. M. Adachi, A. J. Labelle, S. M. Thon, X. Lan, S. Hoogland and E. H. Sargent, *Sci. Rep.*, 2013, **3**, 2928.
3 C. Battaglia, C. Hsu, K. Söderström, J. Escarré, F. Haug, M. Charrière, M. Boccard, M. Despeisse, D. T. L. Alexander, M. Cantoni, Y. Cui and C. Ballif, *ACS Nano*, 2012, **6**, 2790–2797.
4 C. Hsu, C. Battaglia, C. Pahud, Z. Ruan, F. Haug, S. Fan, C. Ballif and Y. Cui, *Adv. Energy Mater.*, 2012, **2**, 628–633, DOI: 10.1002/aenm.201100514.
5 S. E. Han and G. Chen, *Nano Lett.*, 2010, **10**, 4692–4696.
6 H. Huang, L. Lu, J. Wang, J. Yang, S. Leung, Y. Wang, D. Chen, X. Chen, G. Shen, D. D. Li and Z. Fan, *Energy Environ. Sci.*, 2013, **6**, 2965–2971.
7 Q. Lin, H. Huang, Y. Jing, H. Fu, P. Chang, D. Li, Y. Yao and Z. Fan, *J. Mater. Chem. C*, 2014, **2**, 1233–1247.
8 H. Sai, H. Fujiwara, M. Kondo and Y. Kanamori, *Appl. Phys. Lett.*, 2008, **93**, 143501, DOI: 10.1063/1.2993351.
9 R. Yu, Q. Lin, S. F. Leung and Z. Fan, *Nano Energy*, 2012, **1**, 57–72.
10 S. Leung, L. Gu, Q. Zhang, K. Tsui, J. Shieh, C. Shen, T. Hsiao, C. Hsu, L. Lu, D. Li, Q. Lin and Z. Fan, *Sci. Rep.*, 2014, **4**, 4243.
11 V. Shrotriya, E. H. Wu, G. Li, Y. Yao and Y. Yang, *Appl. Phys. Lett.*, 2006, **88**, 064104.
12 Y. Yao, J. Hou, Z. Xu, G. Li and Y. Yang, *Adv. Funct. Mater.*, 2008, **18**, 1783–1789.
13 Y. Qiu, S. Leung, Q. Zhang, B. Hua, Q. Lin, Z. Wei, K. Tsui, Y. Zhang, S. Yang and Z. Fan, *Nano Lett.*, 2014, **14**, 2123–2139.
14 K. H. Tsui, Q. Lin, H. Chou, Q. Zhang, H. Fu, P. Qi and Z. Fan, *Adv. Mater.*, 2014, **26**, 2805–2811, DOI: 10.1002/adma.201304938.
15 K. Cho, D. J. Ruebusch, M. H. Lee, J. H. Moon, A. C. Ford, R. Kapadia, K. Takei, O. Ergen and A. Javey, *Appl. Phys. Lett.*, 2011, **98**, 203101.
16 M. G. Deceglie, V. E. Ferry, A. P. Alivisatos and H. A. Atwater, *Nano Lett.*, 2012, **12**, 2894–2900.
17 M. G. Deceglie, V. E. Ferry, A. P. Alivisatos and H. A. Atwater, *Photovoltaics*, 2013, **3**, 599–604, DOI: 10.1109/jphotov.2013.2240764.
18 Z. Fan, D. J. Ruebusch, A. A. Rathore, R. Kapadia, O. Ergen, P. W. Leu and A. Javey, *Nano Res.*, 2009, **2**, 829–843.
19 J. Grandidier, D. M. Callahan, J. N. Munday and H. A. Atwater, *Adv. Mater.*, 2011, **23**, 1272–1276, DOI: 10.1002/adma.201004393.
20 D. Paz-Soldan, A. Lee, S. M. Thon, M. M. Adachi, H. Dong, P. Maraghechi, M. Yuan, A. J. Labelle, S. Hoogland, K. Liu, E. Kumacheva and E. H. Sargent, *Nano Lett.*, 2013, **13**, 1502–1508, DOI: 10.1021/nl304604y.
21 Y. S. Zhou, K. Wang, W. Han, S. C. Rai, Y. Zhang, Y. Ding, C. Pan, F. Zhang, W. Zhou and Z. L. Wang, *ACS Nano*, 2012, **6**, 6478–6482, DOI: 10.1021/nn3022074.
22 W. Wei, M. Tsai, S. Ho, S. Tai, C. Ho, S. Tsai, C. Liu, R. Chung and J. He, *Nano Lett.*, 2013, **13**, 3658–3663.
23 L. K. Yeh, K. Y. Lai, G. J. Lin, P. H. Fu, H. C. Chang, C. A. Lin and J. H. He, *Adv. Energy Mater.*, 2011, **1**, 506–510.
24 G. Lin, H. Wang, D. Lien, P. Fu, H. Chang, C. Ho, C. Lin, K. Lai and J. He, *Nano Energy*, 2014, **6**, 36–43.

25 R. Kapadia, Z. Fan, K. Takei and A. Javey, *Nano Energy*, 2012, **1**, 132–144.
26 R. Kapadia, Z. Fan and A. Javey, *Appl. Phys. Lett.*, 2010, **96**, 103116.
27 Z. Dong, H. Ren, C. M. Hessel, J. Wang, R. Yu, Q. Jin, M. Yang, Z. Hu, Y. Chen and Z. Tang, *Adv. Mater.*, 2014, **26**, 905–909.
28 H. Tang, C. M. Hessel, J. Wang, N. Yang, R. Yu, H. Zhao and D. Wang, *Chem. Soc. Rev.*, 2014, **43**, 4281–4299.
29 L. Yi, Y. Liu, N. Yang, Z. Tang, H. Zhao, G. Ma, Z. Su and D. Wang, *Energy Environ. Sci.*, 2013, **6**, 835–840.
30 Z. Dong, X. Lai, J. E. Halpert, N. Yang, L. Yi, J. Zhai, D. Wang, Z. Tang and L. Jiang, *Adv. Mater.*, 2012, **24**, 1046–1049.
31 X. Lai, J. E. Halpert and D. Wang, *Energy Environ. Sci.*, 2012, **5**, 5604–5618.
32 J. Du, J. Qi, D. Wang and Z. Tang, *Energy Environ. Sci.*, 2012, **5**, 6914–6918.
33 N. Yang, J. Zhai, D. Wang, Y. Chen and L. Jiang, *ACS Nano*, 2010, **4**, 887–894.
34 R. Guo, H. Huang, P. Chang, L. Lu, X. Chen, X. Yang, Z. Fan, B. Zhu and D. Li, *Nano Energy*, 2014, **8**, 141–149.
35 S. Leung, Q. Zhang, F. Xiu, D. Yu, J. C. Ho, D. Li and Z. Fan, *J. Phys. Chem. Lett.*, 2014, **5**, 1479–1495.
36 M. Heiss, Y. Fontana, A. Gustafsson, G. Wüst, C. Magen, D. O'Regan, J. Luo, B. Ketterer, S. Conesa-Boj and A. Kuhlmann, *Nat. Mater.*, 2013, **12**, 439–444.
37 M. Fickenscher, T. Shi, H. E. Jackson, L. M. Smith, J. M. Yarrison-Rice, C. Zheng, P. Miller, J. Etheridge, B. M. Wong and Q. Gao, *Nano Lett.*, 2013, **13**, 1016–1022.
38 J. Kim, C. Battaglia, M. Charrière, A. Hong, W. Jung, H. Park, C. Ballif and D. Sadana, *Adv. Mater.*, 2014, **26**, 4082–4086.
39 J. Kim, A. J. Hong, J. Nah, B. Shin, F. M. Ross and D. K. Sadana, *ACS Nano*, 2012, **6**, 265–271, DOI: 10.1021/nn203536x.
40 S. Jeong, M. D. McGehee and Y. Cui, *Nat. Commun.*, 2013, **4**, 2950.
41 H. Masuda and K. Fukuda, *Science*, 1995, **268**, 1466–1468.
42 H. Masuda, K. Yada and A. Osaka, *Jpn. J. Appl. Phys.*, 1998, **37**, L1340–L1342.
43 M. J. Naughton, K. Kempa, Z. F. Ren, Y. Gao, J. Rybczynski, N. Argenti, W. Gao, Y. Wang, Y. Peng, J. R. Naughton, G. McMahon, T. Paudel, Y. C. Lan, M. J. Burns, A. Shepard, M. Clary, C. Ballif, F. Haug, T. Soederstroem, O. Cubero and C. Eminian, *Phys. Status Solidi RRL*, 2010, **4**, 181–183, DOI: 10.1002/pssr.201004154.
44 J. Zhu, C. Hsu, Z. Yu, S. Fan and Y. Cui, *Nano Lett.*, 2010, **10**, 1979–1984.
45 J. Li, Y. Qiu, Z. Wei, Q. Lin, Q. Zhang, K. Yan, H. Chen, Z. Fan and S. Yang, *Energy Environ. Sci.*, 2014, DOI: 10.1039/C4EE01581A.
46 Q. Lin, S. Leung, L. Lu, X. Chen, Z. Chen, H. Tang, W. Su, D. Li and Z. Fan, *ACS Nano*, 2014, **8**, 6484–6490.
47 R. Yu, K. Ching, Q. Lin, S. Leung, D. Arcrossito and Z. Fan, *ACS Nano*, 2011, **5**, 9291–9298, DOI: 10.1021/nn203844z.
48 J. Wallentin, N. Anttu, D. Asoli, M. Huffman, I. Aberg, M. H. Magnusson, G. Siefer, P. Fuss-Kailuweit, F. Dimroth, B. Witzigmann, H. Q. Xu, L. Samuelson, K. Deppert and M. T. Borgstrom, *Science*, 2013, **339**, 1057–1060, DOI: 10.1126/science.1230969.
49 Z. Y. Fan, R. Kapadia, P. W. Leu, X. B. Zhang, Y. L. Chueh, K. Takei, K. Yu, A. Jamshidi, A. A. Rathore, D. J. Ruebusch, M. Wu and A. Javey, *Nano Lett.*, 2010, **10**, 3823–3827.
50 R. Gao, Z. Liang, J. Tian, Q. Zhang, L. Wang and G. Cao, *RSC Adv.*, 2013, **3**, 18537–18543.
51 Q. Lin, S. Leung, K. Tsui, B. Hua and Z. Fan, *Nanoscale Res. Lett.*, 2013, **8**, 268.
52 Y. Liao, Y. Wang, Y. Yen, C. Chen, D. Hsieh, S. Chen, C. Lee, C. Lai, W. Kuo and J. Juang, *ACS Nano*, 2013, **7**, 7318–7329.
53 C. Genet and T. W. Ebbesen, *Nature*, 2007, **445**, 39–46, DOI: 10.1038/nature05350.
54 S. F. Leung, M. Yu, Q. Lin, K. Kwon, K. L. Ching, L. Gu, K. Yu and Z. Fan, *Nano Lett.*, 2012, **12**, 3682–3689.
55 Q. Lin, B. Hua, S. Leung, X. Duan and Z. Fan, *ACS Nano*, 2013, **7**, 2725–2732.
56 C. Koch, M. Ito and M. Schubert, *Sol. Energy Mater. Sol. Cells*, 2001, **68**, 227–236.
57 M. H. Lee, N. Lim, D. J. Ruebusch, A. Jamshidi, R. Kapadia, R. Lee, T. J. Seok, K. Takei, K. Y. Cho, Z. Y. Fan, H. Jang, M. Wu, G. J. Cho and A. Javey, *Nano Lett.*, 2011, **11**, 3425.
58 M. Haque, H. Naseem and W. Brown, *Sol. Energy Mater. Sol. Cells*, 1996, **41**, 543–555.
59 J. Arch, F. Rubinelli, J. Hou and S. Fonash, *J. Appl. Phys.*, 1991, **69**, 7057–7066.
60 S. S. Hegedus, *The open circuit voltage of amorphous silicon pin solar cells*, IEEE, 1988.
61 M. Isomura, T. Takahama, S. Tsuda and S. Nakano, *Jpn. J. Appl. Phys.*, 1993, **32**, 1902–1907, DOI: 10.1143/jjap.32.1902.

